



Synthesis and Characterization of Novel Chitosan/Graphene Oxide/Poly (Vinyl Alcohol) Aerogel Nanocomposite for High Efficiency Uranium (VI) Removal from Wastewaters

Mohammed D. Majeed¹ · Mahmoud Roushani¹

Received: 9 September 2023 / Accepted: 31 October 2023 / Published online: 30 November 2023
© The Author(s), under exclusive licence to Springer Science+Business Media, LLC, part of Springer Nature 2023

Abstract

The toxic and the hazardous ramifications that affect both the environment and human beings due to the existence of uranium in wastewater are a huge challenge towards a sustainable environment. Uranium removal from wastewater is a big difficulty that is becoming more severe as the world's population grows and energy demand rises. A hydrothermal and freeze-drying process is used to create a chitosan/graphene oxide/poly (vinyl alcohol) aerogel (CH/GO/PVA) for a very effective and selective uranium removal. Batch experiments were used to examine hexavalent uranium (VI) sorption from wastewater. The efficiency of U (VI) removal was investigated for time of contact, various pH, dosage of sorbent, initial concentration of U (VI), and temperature values. Field emission scanning electron microscopy, Fourier transform infrared spectroscopy, Energy Dispersive Spectroscopy, X-ray diffraction, and Brunauer-Emmett-Teller are utilized to describe the composition, morphology, polymer formation and nanocomposites. Kinetic and Freundlich equations, and the pseudo-second-order are used to illustrate the adsorption process. The adsorption capacity of U (VI) reaches its maximum of 1247 mg g⁻¹ when an initial uranium concentration is 380 mg L⁻¹, and the highest uranium removal efficiency is 98.44%. Thermodynamic study reveals an endothermic and spontaneous adsorption mechanism. Furthermore, the as-synthesized GO/CS/PVA aerogel has good mechanical as well as thermal stability, and can be utilized six times before losing a substantial portion of its original removing effectiveness.

Keywords Graphene oxide · Chitosan · Poly (vinyl alcohol) · Adsorption · Uranium ions

Introduction

Uranium is utilized in numerous areas of science and technology is extremely beneficial; but, its usage generates radioactive waste, which endangers the environment and human beings [1]. Uranium is an essential component in producing nuclear energy, though the wastewater contamination is caused by uranium ore mining activities [2]. The presence of uranium has devastating impact on all ecological systems, and it might transfer radiotoxicity to humans through food cycles. Uranium concentrations which contaminate water close to mine and manufacturing sites can reach hazardous levels, while natural water has lower concentrations. The

techniques used for removing uranium from wastewater are supposed to be extremely selective and economic, and they should possess a high efficiency to recover uranium that minimizes the impact of radioactive and chemical pollution [3]. Standard uranium removal methods, including the process of reverse osmosis [4], solvent extraction [5], ions exchange [6], precipitation [7], photoreduction [8] and sorption by numerous synthetic materials [9], have demonstrated outstanding effectiveness in eliminating uranium from contaminated wastewaters. Latest developments in nanomaterials have created numerous potentials for the exploration and application of more effective radioactive wastewater purification methods. Graphene oxide (GO)-based nanomaterials have garnered considerable attention due to the special physicochemical features like great chemical stability, functional groups containing a lot of oxygen, and high specific surface area- [10–12]. These benefits make GO-based nanoparticles desirable options for uranium adsorption. As a result, multiple investigations attempt to increase the U(VI)

✉ Mahmoud Roushani
m.roushani@ilam.ac.ir; mahmoudroushani@yahoo.com

¹ Department of Chemistry, Faculty of Sciences, Ilam University, P. O. BOX, Ilam 69315-516, Iran

performance in adsorbing by modifying GO using different functional groups that include as phosphate, amines, polydopamine, amidoxime and, chitosan. Chitosan (CS) has gained much attention due to its qualities and potential applications. The papers and applications using this polymer increases annually. Chitosan is not easily soluble in neutral and basic media, restricting its usage in those circumstances. An additional significant constraint is related natural origin of it. Monomer distribution, size, and composition of Chitosan can be modified which distinguishes it from being a single polymer with a specified structure. These attributes have considerable impact on the polymer's biological and technological functionality [13, 14]. The amino groups protonation along the chitosan is caused by the dissolution of CS in aqueous acids, resulting in the formation of cationic sites. This distinct characteristic improves CS's solubility, polarity, and ability to adsorb various contaminants. Protonated amine groups can attract metal anions [15]. Natural organic biopolymers molecules created via renewable materials and sources and living organisms, are regarded to be greener, more sustainable, and safer for the environment. Natural polysaccharides are considered eco-friendly because they are available, nontoxic, biocompatible, and modified easily and have favorable applications. Lately, numerous polysaccharides are used to develop several (nano) catalysts; manufacture of polysaccharides which support metal/metal oxide materials is an practicable method in nanotechnology [16]. Poly vinyl alcohol, is a thermoplastic synthetic polymer that, in contrast to the vast majority of other synthetic ones, is produced by hydrolyzing poly vinyl acetate. Hydrophilic polymers are utilized to synthesize hydrogels with distinct morphological and physicomechanical characteristics such as PVA and its composites that are comprised mostly of biopolymers. PVA hydrogels and other composites of PVA are investigated due to their multiple applications in membranes made of electrical film that are used for separating chemicals and dye removal, fuel cells, metal ion adsorption and packaging [17–19]. Aerogel (AG) is a porous ultra-light material developed from gelly substrates in which the gel is substituted with gas, resulting in a solid with extremely low temperatures dissipation conduct and low density because of its 99.8% air composition. The advancement of nanotechnology has made it possible to integrate dissipation conduct into nanomaterials like graphene and carbon nanotubes, within AG, leading to the production of light-weight, efficient, and multi-purpose aerogel nanoarchitectures [20, 21]. Graphene aerogels are highly porous, and highly compressible and possess a large specific surface area, and low density. The combination of these unique factors has led to considerable interest in a variety of implementations, including attenuating exceptional efficiency electromagnetic wave. The Gas interior structure porosity and the three-dimensional network are the solution to the graphene sheet layer aggregation,

highly conductive, and inaccurate impedance existing in two-dimensional graphene, which improves microwave absorption capacity [22–24]. Thus, this paper aims at evaluating the role of GO in the progress of a versatile sorbent composite system capable of adsorbing uranium from aqueous solutions. Hydrothermal and lyophilization treatments are implemented to improve the adsorption capacity and hydrophobicity of graphene oxide, chitosan, and Poly (vinyl alcohol). To mitigate its hazardous properties, even at low amounts, uranium-contaminated water must be treated before being discharged. Sorbent dose, temperature, pH, time of contact, and initial ion concentration of uranium are all investigated. Langmuir and Freundlich isotherm models are utilized to fit adsorption data. The adsorption kinetic mechanism of uranyl ion UO_2^{2+} is studied using pseudo-1st and pseudo-2nd order models. Thermodynamic parameters are calculated as well, with the main parameters of free energy, enthalpy, and entropy change estimated. The morphology and characteristics of the composite are assessed by FE-SEM/EDS, XRD, FTIR, and BET characterization techniques.

Materials and Methods

Materials

Graphite Powder of 99.99 wt % purity was provided by Sigma -Aldrich, USA. The graphene oxide is produced using the modified Hummer's technique. Chitosan (Glentham Life Sciences, UK). Poly (vinyl alcohol) (PVA) manufactured by (Panreac, Spain). Potassium permanganate (KMnO_4) is purchased from BDH, UK. 1 g L^{-1} U (VI) stock solution is prepared by dissolving of $\text{UO}_2(\text{NO}_3)_2 \cdot 6\text{H}_2\text{O}$ Sigma-Aldrich with deionized water. All chemical reagents, sulfuric acid, hydrochloric acid, phosphoric acid, sodium hydroxide and hydrogen peroxide are analytical grades and purchased from (Sigma Aldrich, USA). Deionized water ($18.0 \text{ M}\Omega \text{ cm}$) is utilized to prepare solutions in the experiments.

Preparation of GO/CS/PVA

The modified Hummer's method is used to synthesize graphene oxide from pure graphite powder [25]. 360 mL of sulfuric acid and 40 mL of phosphoric acid (volume ratio 9:1) are combined and stirred much in this method. Then, 3 g of graphite powder is poured into the mixed solution while stirring. The solution is then gradually supplemented with 18 g of potassium permanganate (KMnO_4). This solution is stirred for a period of 6 h until it turned dark green. Removing the excess (KMnO_4), 3 mL of hydrogen peroxide is gradually added and stirred for 12 min. After the exothermic reaction took place, the temperature was granted time

to gradually decrease. 10 mL of hydrochloric acid and 30 mL of deionized water are added and centrifuged for 7 min at 6000 rpm in an Eppendorf Centrifuge. The supernatant is then decanted, and HCl 30% and DIW are used to rewash the residuals three times. Producing the GO powder requires drying the purified GO solution in an oven at 90 °C for 24 h. The dried GO of 0.4 g and PVA of 0.4 g are ultrasonically dispersed in 30 mL 2% acetic acid for 2 h before being combined with 20 mL of (0.8 g) CS solution also in 2% acetic acid. The GO/CS/PVA suspension is then transferred to a 20 mL syringe (needle diameter: 0.8 mm) and injected at a controlled rate of 5 mL/h into a 1 M NaOH solution. GO/CS/PVA hydrogel beads are repeatedly rinsed with deionized water (at least four times), then vacuum freeze-dried for 72 h.

Batch Adsorption Experiment

In adsorption investigations, GO/CS/PVA aerogels (15 mg) are added into U(VI) solution (50 mL). Adsorption experiments were conducted at different conditions, Sorbent Dose (5–20 mg), pH (3, 4, 5, 6, 7, 8), contact time (1–24 h), temperature (293–313 K), initial U(VI) concentration (50–400 mg L⁻¹) and reusability of adsorbent. The mixtures were shaken on an overhead shaker. After 14 h of adsorption, the adsorbent is extracted by centrifugation to separate the solid and liquid phases. An Energy Dispersive X-ray Fluorescence (EDXRF) (Rigaku, USA) is utilized to measure the absorbance of residual U(VI). The average of triple measurements is used to determine all batch data. The adsorption capacity (Q_e) and removal efficiency (R) are calculated by the following equations:

$$\text{Adsorption capacity} = [(C_0 - C_e)/m] \times V \quad (1)$$

$$\text{Removal efficiency} = [(C_0 - C_e)/C_0] \times 100\% \quad (2)$$

where C₀ and C_e are the initial and equilibrium uranium concentrations, respectively, V (mL) is the uranium solution volume, and m (mg) is the amount of GO/CS/PVA aerogel.

Characterization

Following the successful synthesis of the nanocomposite using the post-functionalization procedure, it is comprehensively characterized utilizing several physicochemically defined technical analysis like Fourier Transformed Infrared Spectroscopy (FT-IR) spectra are gathered utilizing pressed (KBr) pellets on a Shimadzu 8400S infrared spectrometer in the 400–4000 cm⁻¹ span. Field emission scanning electron microscopy (JEOL JSM-6330F, JAPAN), Energy Dispersive X-ray Electron Spectroscopy, Brunauer-Emmett-Teller and X-ray diffraction pattern of the synthesized materials are

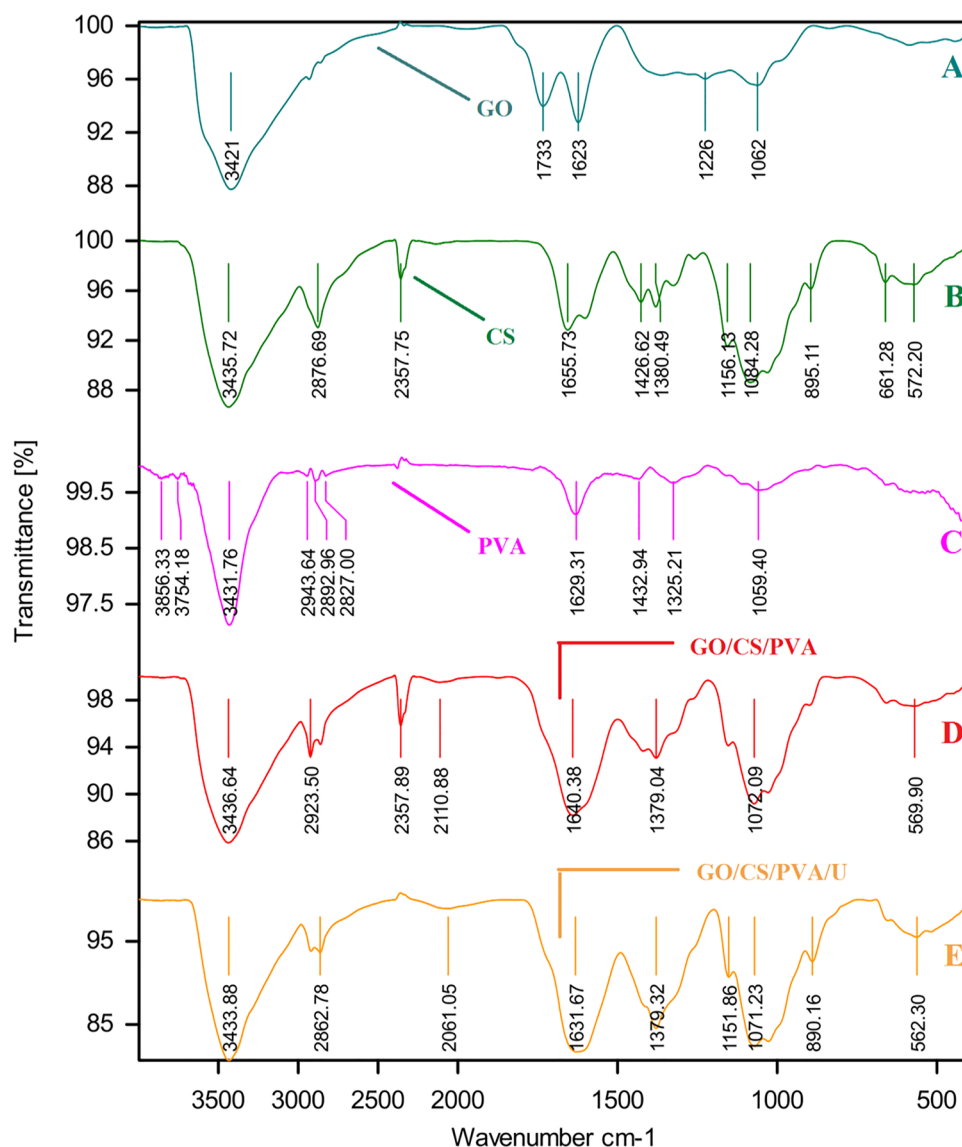
carried out utilizing a Bruker D8 Advance powder X-ray diffractometer with Cu Kα (λ = 0.15406 nm) radiation over the diffraction angle (2θ) of (10°–80°). After pre-treatment, the pore surface qualities of the finalized samples are measured in an adsorption-desorption test using a MicrotracBEL Belsorp-max porosity analyser with N₂ by 99.9999% purity at 77 K. The Brunauer-Emmett-Teller method is employed for calculating the specific surface area (S_{BET}), total pore volume (S_{total}), and mean pore diameter of ACNFs. The micropore volume (S_{micro}) of ACNFs is calculated using the BELSORP analysis program software's t-plot and Barrett-Joyner-Halenda (BJH) methodologies. All pore size distribution and S_{BET} and characterizations of the final ACNF samples from N₂ adsorption-desorption experiments are carried out in at least triplicate.

Result and Discussion

Characterization of GO/CS/PVA Aerogel

GO FTIR spectrum in Fig. 1A depicts a wide peak in the frequency area of 3421 cm⁻¹ corresponding to (OH) groups of water molecules stretching and bending vibration adsorbed on graphene oxide. Other bands observed at 1733 cm⁻¹ are there due to stretching vibrations (C=O) of the COOH group corresponding to carbonyl and carboxyl groups, 1623 cm⁻¹ to in-plane vibration (C=C) from un-oxidized sp² CC bonds, 1226 cm⁻¹ to epoxy (C–O) vibrations, and 1062 cm⁻¹ to stretching vibrations (C–O) of the alkoxy group [26, 27]. Figure 1B depicts the FTIR spectrum of chitosan. A distinctive band at 3435 cm⁻¹ is related to stretching of O–H, the band at 2876 cm⁻¹ to that of (C–H), and the band at 1655 cm⁻¹ to N–H bending for (NH₂) [28]. PVA FTIR spectra in Fig. 1C depict all the crucial peaks related to groups of hydroxyl and acetate. The broad band noticed at 3431 cm⁻¹ is because of the stretching of (OH) from inter- and intramolecular hydrogen bonding. The alkyl groups (C–H) stretching is indicated by the observed peak at 2943.2827 cm⁻¹, moreover, the residual acetate groups in PVA generate the peak at 1629 cm⁻¹ due to (C=O) stretching. The (C–H) bending peak emerges at 1325 cm⁻¹. The stretching peak of (C–O) emerges at 1059 cm⁻¹ [29]. In Fig. 1D, the (O–H), (C–H) and (C=O) FTIR peak stretching vibrations are all changed to higher frequencies after adding the PVA for the GO/CS/PVA, indicating the hydroxyl group (–OH) and the amino group (–NH₂) strong interactions of the CS after adding the PVA, and indicated that the GO/CS/PVA aerogel is successfully synthesized [30]. The FTIR spectra obviously shifted after saturation adsorption. Since the peak of the GO/CS/PVA framework is very stable, this suggests that the U(VI) adsorption did not significantly alter the framework's structure. In Fig. 1E the adsorption peaks at nearly 2950

Fig. 1 FTIR spectra of GO (A), CS (B), PVA (C), GO/CS/PVA (D) and GO/CS/PVA/U (E)



cm^{-1} shifted to 2820 cm^{-1} and became feeble. The results point that (C–H), (C=C), ($-\text{CH}_2\text{CH}_3$), (C–N–H), and other groups are included in the exchange adsorption manner of U(VI). The peak appeared at 890 cm^{-1} and is greatly strengthened, indicating that it is the uranium adsorption peak [31, 32]. This asserts the reaction between GO/CS/PVA aerogel and uranium ions U(VI) in wastewater [33].

The X-ray diffraction spectra of GO, GO/CS/PVA aerogel, and GO/CS/PVA-U are shown in Fig. 2. The XRD spectra of GO is revealed in diffraction sharp peaks at 11.2° , which corresponds to the typical peak of GO [34]. The chain interaction of PVA and CS polymers influences physical properties including polymer solubility, crystallinity, ion exchange capacity, thermal and chemical stability. The mechanical characteristics and crystallinity can be correlated. The X-ray diffractograms spectra of chitosan-containing blends as well show a significant diffraction peak close

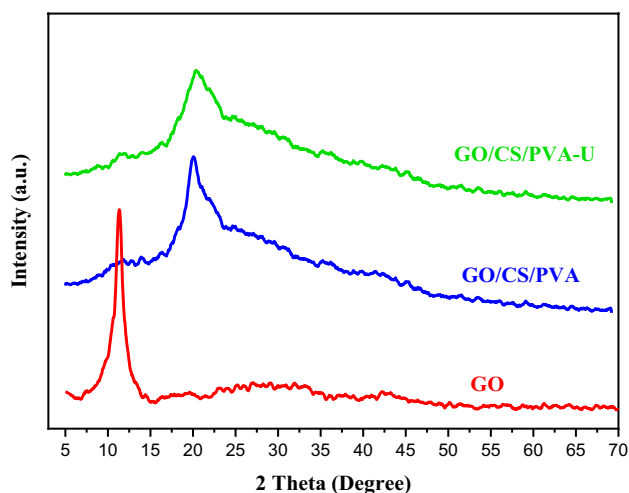


Fig. 2 The (XRD) patterns of GO, GO/CS/PVA and GO/CS/PVA-U aerogels

to 20°. Because the chitosan primary diffraction peak arises near 20°, similarly to PVA, this peak's intensity shows the crystalline degree of PVA and chitosan phases [35]. After adding the GO filler, the semi-crystalline structure of the CS/PVA mix is diminished; nevertheless, the unique diffractogram bands associated with main polymers can still be seen in the GO/CS/PVA aerogel. When compared to the CS/PVA mix, the GO/CS/PVA aerogel presents slightly wider bands. As a result, the GO's incorporation into the matrix of the polymer causes a minor loss of crystallinity, as documented in different layer filler additives. Both amorphous and crystalline areas have a positive influence on the aerogel's electrical and mechanical characteristics. As a consequence of this, the GO/CS/PVA is still almost crystalline. The (XRD) results match with those gathered, indicating that the introduction of GO and its derivative sheets decreased the crystallinity of CS/PVA, expanding the relative full width at half maximum (FWHM) value as carbon filler concentration increased. Although, the preparation technique, including temperature and crosslinking agents, can affect the degree of crystallinity, so it's important to consider the fact that the ratio of CS to PVA polymers and carbon filler varies. When the uranium is adsorbed, the Peak-Shifting and its intensity decrease slightly.

Figure 3 shows how the surface morphologies are studied by field emission scanning electron microscopy before and after U(VI) adsorption. As Fig. 3A shows, the surfaces of GO/CS/PVA aerogel possess a fine three-dimensional network structure, resulting in a porous structure, and the GO sheets are layered and arranged, resulting in increased surface area for adsorption and helps to attain an enhanced adsorption result [30]. Figure 3B shows that the aerogel composite's surface has a very porous structure that is actively adsorbing uranium.

For both GO/CS/PVA aerogel and GO/CS/PVA-U(VI)-loaded, elemental mapping and SEM/EDS analysis of the surface morphologies are performed. According to the EDS examination depicted in Fig. 4B U(VI) ions are successfully adsorbed with a high capacity onto the GO/CS/PVA aerogel. Figure 4A shows that the SEM with EDS spectra of the aerogel's main components, C, O, and N. Furthermore, the mapping images clearly show that uranium is uniformly distributed in the nanocomposite aerogels.

The Analysis of the Brunauer–Emmett–Teller (BET)

The Brunauer–Emmett–Teller method has been utilized to investigate the porosity and specific surface area. The obtained N₂ adsorption-desorption isotherms of the GO/CS/PVA Fig. 5A, and GO/CS/PVA with adsorbed uranium Fig. 5B can be seen. In addition, results of pore size distribution related to materials using the Barrett–Joyner–Halenda method can be seen in the inset of each isotherm. As expected, the two samples' BET surface area reduced in the following order: GO/CS/PVA (14.19 m² g⁻¹) > GO/CS/PVA with adsorbed uranium (9.84 m² g⁻¹). This decrease is caused by the absorption of uranium on GO/CS/PVA. As can be seen, the isotherm curves were of type IV, which confirmed the existence of mesoporous structures [36]. Additionally, in the comparatively high-pressure region, obvious hysteresis loops are shown, which shows the existence of mesoporous. The total pore volume of GO/CS/PVA and GO/CS/PVA with adsorbed uranium is estimated to be 0.0087 and 0.0066 cm³/g, respectively. From the SEM morphology of GO/CS/PVA (Fig. 3A and B), the pore structure morphology of them is roughly similar. Lots of pores with different sizes cross-linked with each other to form a faveolated porous network structure. The samples' BJH average pore size

Fig. 3 FE-SEM images of GO/CS/PVA aerogel (A) and GO/CS/PVA-U (B)

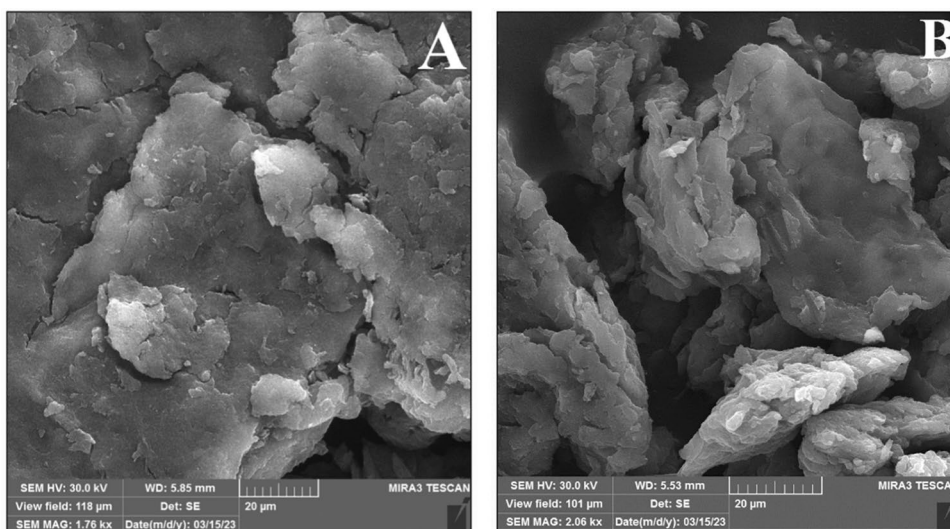
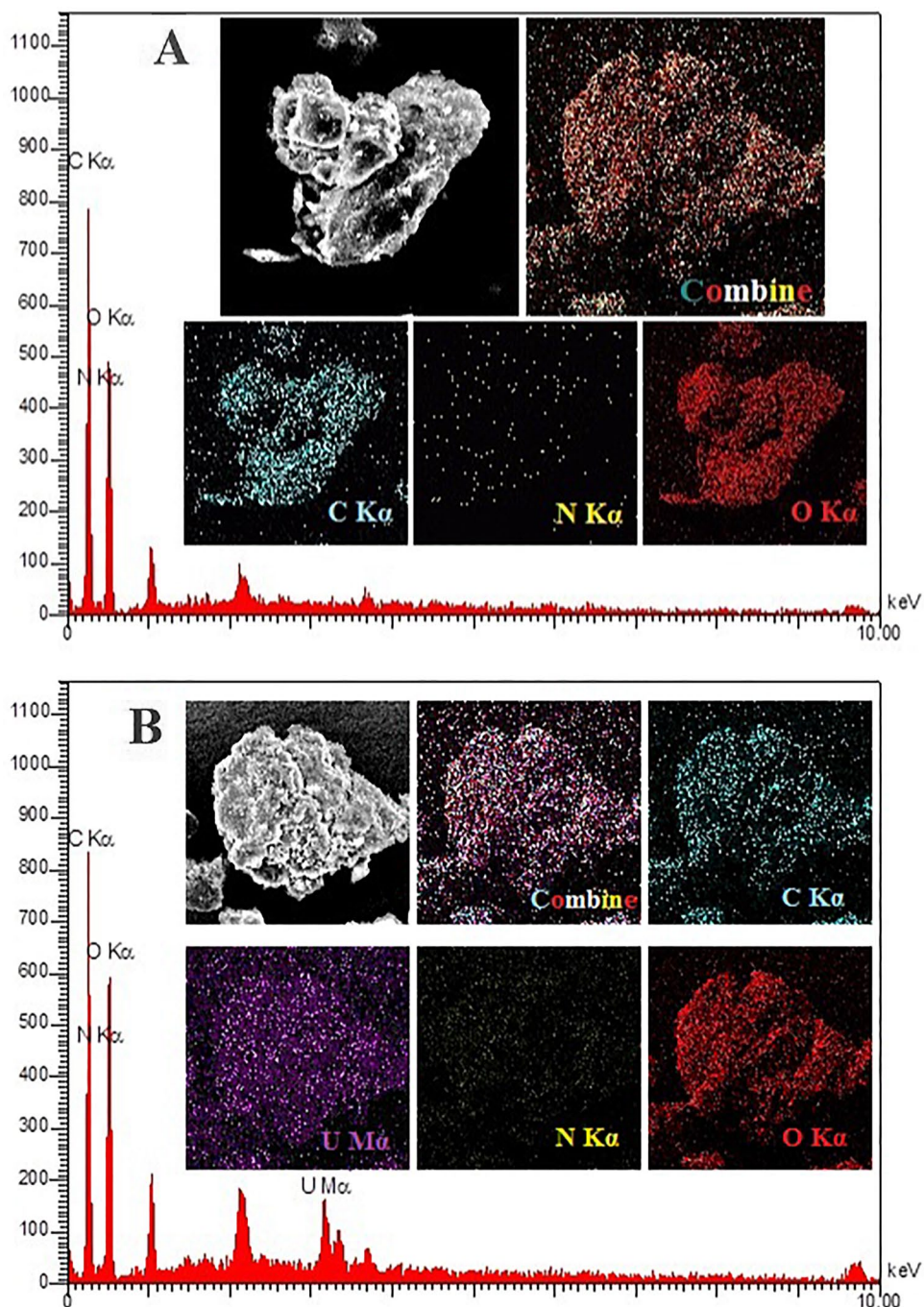


Fig. 4 Elemental mapping and SEM/EDS spectra of GO/CS/PVA aerogel. **A** Before adsorption and elemental mapping and SEM/EDS spectra of GO/CS/PVA-U(VI)-loaded **B** after adsorption



distribution was in the range of 2–50 nm which confirmed the mesoporous structure.

Adsorption Behavior of U(VI) on GO/CS/PVA

Effect of Sorbent Dose

The sorbent's removal efficiency is determined by the sorbent amount. The metal extraction percentage

increases as sorbent quantity increases. Due to increases the effective surface area of the nanomaterial with the increase of the mass of aerogels. The adsorbent dose measurement provides an indication of how much sorbent is required for the sorption process. Adsorption capacities (Q_e) are examined in Fig. 6 by using different quantities of adsorbent ranging from (5 to 20) mg. The maximum removal would occur with 15 mg of adsorbent.

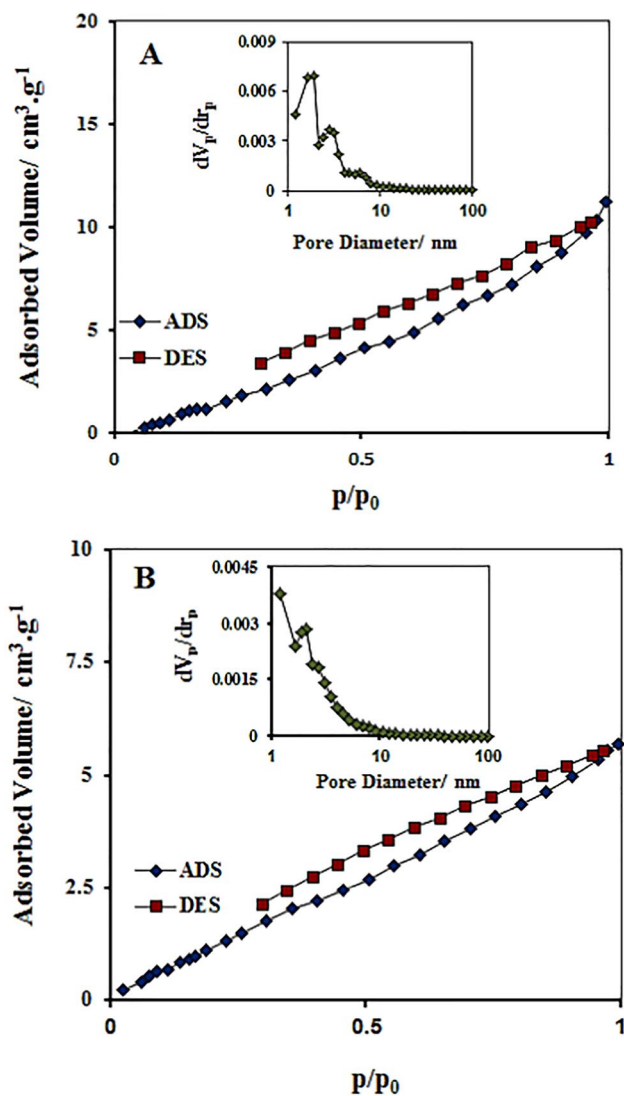


Fig. 5 The obtained N₂ adsorption-desorption isotherms of A GO/CS/PVA, and B GO/CS/PVA with adsorbed uranium; (inset: related BJH pore-size distribution curve of samples)

Effect of pH on Adsorption

Adsorption is very sensitive to changes in the mixture’s pH. It influences the adsorption of metal ion on the adsorbent. The solution’s pH influence can be illustrated through changing the loads of surface and ionizing degree of the metal ions in an aqueous solution. Consequently, assessing the pH effect on adsorption is critical. The pH solutions of uranium concentration was adjusted by adding 0.1 M HNO₃ or 0.1 M NaOH solution. Figure 7 depicts the pH effects on U(VI) adsorption by GO/CS/PVA aerogel. In this experiment, the effects of pH value (pH = 3, 4, 5, 6, 7, 8) T = 313 K, t = 24 h, C₀ = 200 mg L⁻¹, and mass of GO/CS/PVA aerogel = 15 mg on the adsorption property of uranium are examined. The

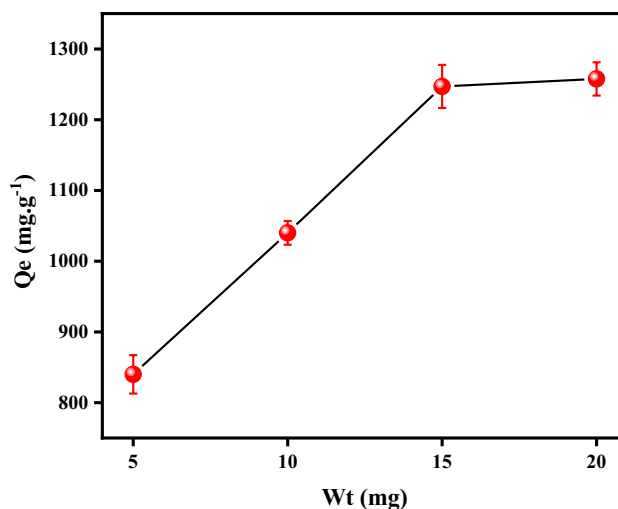


Fig. 6 Effect of GO/CS/PVA aerogel dosage on the adsorption of U(VI) pH=6, contact time 24 h, initial U(VI) concentration 550 mg L⁻¹, temperature 313 K

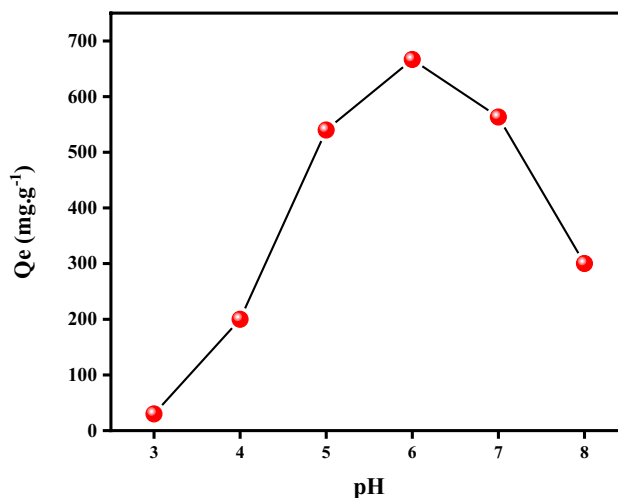


Fig. 7 Effect of pH on adsorption capacity of U(VI) mass of GO/CS/PVA aerogel =15 mg, contact time 24 h, initial U(VI) concentration 200 mg L⁻¹, temperature 313 K

adsorption capacity elevated rapidly from (3.0 to 6.0) pH, then gradually decreased for pH values greater than 6.0. Results may be explained by the relative distribution of U(VI) species and changes in adsorbent surface charge over a range of pH values. At high pH, U(VI) mostly persisted as the positively charged cations UO₂⁺ and (UO₂)₃(OH)₅⁺, which are electrostatically repelled by the negatively charged surface of GO/CS/PVA. U(VI) adsorption capacity is enhanced since the electrostatic repulsion between GO/CS/PVA and U(VI) is significantly reduced. When the pH increased above 6.0, the measurements of UO₂(OH)³⁻ and (UO₂)₃(OH)⁷⁻ formed from the hydrolysis

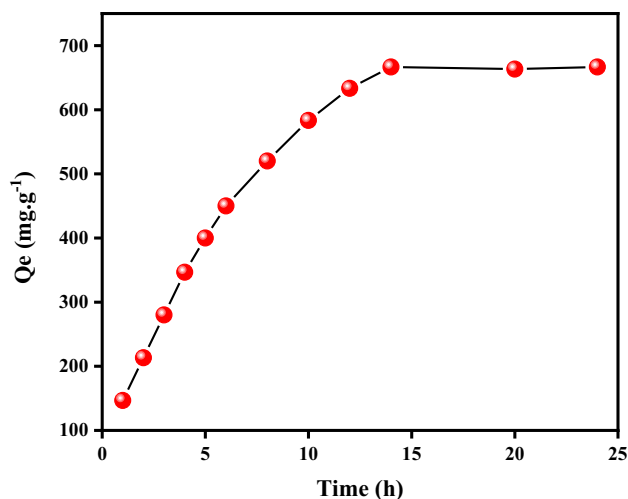


Fig. 8 Effect of contact time on adsorption capacity of U(VI) mass of GO/CS/PVA aerogel =15 mg, pH=6, initial U(VI) concentration 200 mg L⁻¹, temperature 313 K

Table 1 Kinetic parameters of uranium adsorption onto GO/CS/PVA aerogel

	Pseudo-first-order kinetic		
	k1 (h ⁻¹)	Q _{e,cal} (mg g ⁻¹)	R ²
Q _{e,exp} (mg g ⁻¹) 666.66	0.3044	956.42	0.8675
	Pseudo-second-order kinetic		
	k2 (g mg ⁻¹ h ⁻¹)	Q _{e,cal} (mg g ⁻¹)	R ²
	0.000232	833.33	0.9872

of U(VI) increased, strengthening the negative charge on the GO/CS/PVA surfaces that repels these anions.

Effect of Contact Time and Sorption Kinetics Studies

Experiments are executed to examine the impact of the performance of GO/CS/PVA aerogel and adsorption time ($t = 1\text{--}24$ h, $C_0 = 200$ mg L⁻¹, $T = 313$ K, mass GO/CS/PVA =15 mg, pH = 6.0). As demonstrated in Fig. 8, the GO/CS/PVA aerogel adsorptive capacity for uranium improves with adsorption time and achieves equilibrium after 14 h. The curve shows that the GO/CS/PVA adsorption capacity for uranium increases significantly, which is because of a large number of adsorption sites' presence on the material's surface at the beginning of the reaction, leading to more and more uranium (VI) binding on the material's surface. By the progress of the reaction, uranyl ions little by little covered the adsorptive spots on the materials' superficies, and the adsorptive process eventually reached equilibrium. Two distinct kinetic models, pseudo-first order and pseudo-second order are utilized to test the sorption process the mechanism. Table 1 illustrates the pseudo-second-order kinetics equation

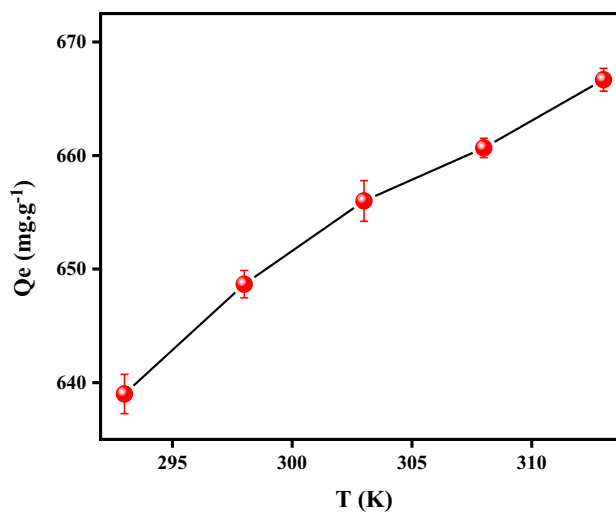


Fig. 9 Effect of temperature on adsorption capacity of U(VI) mass of GO/CS/PVA aerogel =15 mg, pH=6, initial U(VI) concentration 200 mg L⁻¹, contact time 24 h

Table 2 The thermodynamic parameters for adsorption of uranium (VI) by GO/CS/PVA aerogel

ΔH° (kJ mol ⁻¹)	ΔS° J (mol K) ⁻¹	ΔG° (kJ mol ⁻¹)	
82.760	310.952	-10.3991	293 (K)
		-11.9889	298 (K)
		-13.5787	303 (K)
		-15.1684	308 (K)
		-16.7582	313 (K)

for the adsorption of U(VI) by GO/CS/PVA aerogel, the adsorption curves on the GO/CS/PVA surface are linear, and the Q_e (cal) is closer to the experimental value. As a result, the process of uranium (VI) adsorption follows the pseudo-second-order equation, which states that the reaction is essentially regulated by chemical action.

Effects of Temperature and Thermodynamic Analysis

Figure 9 depicts how temperature affects the U(VI) adsorption on GO/CS/PVA aerogel. The effectiveness of U(VI) adsorption increased as temperatures raised from 293 to 313 K, implying that higher temperature promotes U(VI) adsorption on GO/CS/PVA aerogel. Table 2 and Fig. 9 show the determined thermodynamic parameters. The presence of a positive value of ΔH° 82.760 kJ mol⁻¹ demonstrated that U(VI) adsorption on GO/CS/PVA aerogel is an endothermic process in nature [37]. The positive ΔS° 310.952 J (mol K)⁻¹ displays the increased randomness during the sorption phase at the solid-solution contact. The negative value of ΔG° reduced with raising temperature, from (-10.3991 to

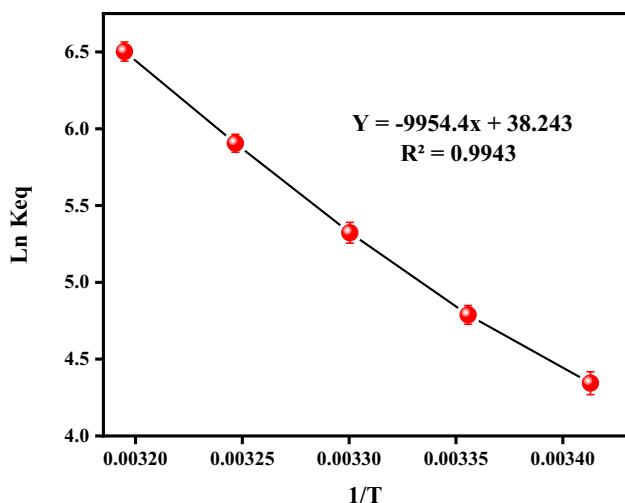


Fig. 10 Plot between equilibrium constant and temperature invers to calculate thermodynamic functions for U(VI) on GO/CS/PVA aerogel

-16.7582) kJ mol⁻¹, demonstrating that the adsorption process occurs spontaneously and is more effective at elevated temperatures [38]. Figure 10 shows plot between equilibrium constant and temperature invers to calculate thermodynamic functions for U(VI) on GO/CS/PVA aerogel.

The alteration in thermodynamic parameters of the sorption phase is calculated using Eq. (3).

$$\text{Ln } K_{\text{eq}} = \frac{-\Delta H}{RT} + \frac{\Delta S}{R} \tag{3}$$

K_{eq} is the distribution coefficient (mL/g), R is the gas constant 8314 J (mol K)⁻¹ and T is the absolute temperature (K). ΔS° is the change in entropy J (mol K)⁻¹ and ΔH° is the change in enthalpy (kJ mol⁻¹). Equation (4) provides the change in Gibbs free energy (ΔG°) values (kJ mol⁻¹).

$$\Delta G^\circ = \Delta H^\circ - T\Delta S^\circ \tag{4}$$

Effects of Initial U(VI) Concentrations and Isotherm Models

Adsorption processes require and rely on equilibrium isotherm studies to predict the behavior of U(VI) ions adsorption onto adsorbent surfaces. Batch studies are used to investigate the influence of initial uranyl ion content on the adsorption of GO/CS/PVA aerogel ($C_0 = 50\text{--}400$ mg L⁻¹, mass GO/CS/PVA =15 mg, $T = 313$ K, $t = 24$ h, $\text{pH} = 6.0$). As Fig. 11 shows, the adsorptive quantity of GO/CS/PVA aerogel for U(VI) increases by degrees as the initial content of U(VI) in the solution increases. Langmuir and Freundlich models, describe homogeneous and heterogeneous adsorption. The Langmuir isotherm is an empirical model in which adsorption manifests at identical

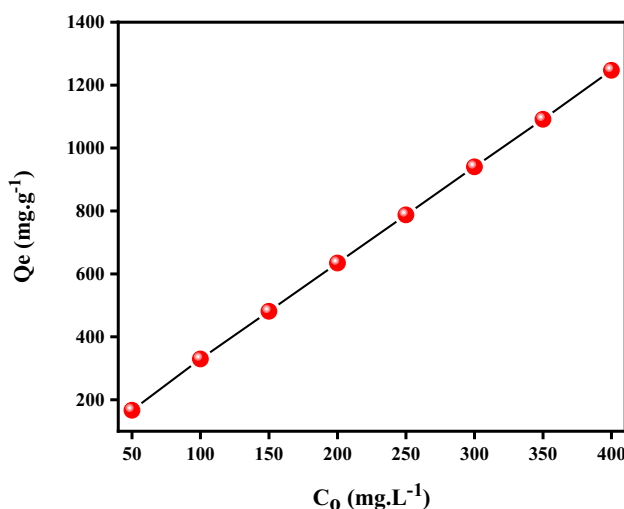


Fig. 11 Effects of initial concentration on adsorption capacity for GO/CS/PVA aerogel mass of GO/CS/PVA aerogel =15 mg, pH=6, contact time 24 h, temperature 313 K

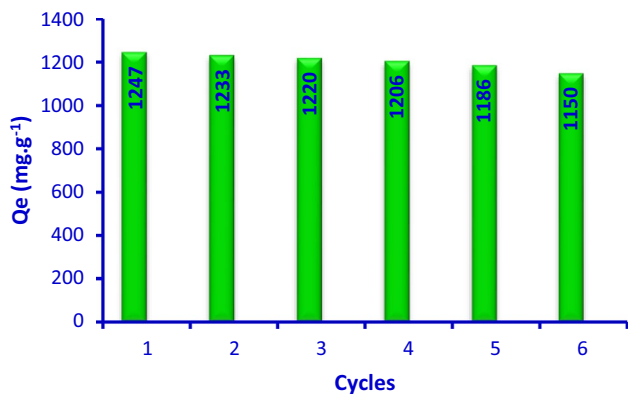
and equivalent definite localized spots and the thickness of the adsorbed layer is one molecule (monolayer adsorption). The reversible and non-ideal adsorption process is described by the Freundlich adsorption isotherm model. Unlike the Langmuir isotherm model, the Freundlich model is not limited to monolayer formation and can be applied to multilayer adsorption [39]. As shown in Table 3, the fitting coefficient R^2 of Langmuir is greater than the R^2 of Freundlich, implying that the former is more in agreement with the adsorptive process. The experimental data demonstrated that the behavior of adsorption of the GO/CS/PVA aerogel is mostly monolayer adsorption, and the maximal adsorptive quantity predicted by the Langmuir equation is 1247 mg g⁻¹.

Reusability

Reusability of adsorbent is necessary for commercial applications. The adsorption capacity of U(VI) slightly decreased from 1247 to 1150 mg g⁻¹ after six cycles Fig. 12, suggesting GO/CS/PVA aerogel has good recycling adsorption of U(VI) performance. In addition, the U(VI) desorption rate decreased slightly after six cycles Fig. 12, confirming that GO/CS/PVA can be rapidly regenerated with the conventional acidic solution. Furthermore, the nanocomposite as synthesized is insoluble and can be separated from the reaction mixture through simple centrifugation. Consequently, GO/CS/PVA aerogel may have the ability to remove U(VI) from wastewaters in practical applications.

Table 3 Langmuir and Freundlich isotherm for adsorption of U(VI) on GO/CS/PVA aerogel

Sorbent GO/CS/PVA aerogel	Langmuir sorption isotherm			Freundlich sorption isotherm		
	Q_{\max} (mg g ⁻¹)	K_L (L mg ⁻¹)	R^2	K_F [(mg g ⁻¹) (L mg ⁻¹) ^{1/n}]	n	R^2
	1247	2.7090	0.9816	219.3788	1.9825	0.9282

**Fig. 12** Reusability for GO/CS/PVA aerogel

Conclusions

In this study, we used a freeze-drying approach to successfully synthesis a 3D porous GO/CS/PVA aerogel to remove Uranyl ion (VI) from aqueous solutions. When the mass of GO/CS/PVA aerogel is 15 (mg), the pH is 6, the temperature is 313 K, and the time is 14 h, the adsorptive capacity of GO/CS/PVA aerogel for uranyl ions is 1247 mg g⁻¹. To match experimental data well, the Langmuir model and second-order kinetic model are applied. The maximal adsorption capacity calculated is relatively comparable to the experimentally obtained data. According to the thermodynamic data derived from the adsorption isotherms, adsorption is an endothermic and spontaneous process. Furthermore, GO/CS/PVA aerogel offers the characteristics of cheaper cost, reusability, and an easy operation method, making it a suitable adsorption material for dealing with uranium-contaminated wastewater and reducing environmental pollution.

Author Contributions MDM: Resources, investigation, methodology, validation, funding acquisition roles/writing—original draft. MR: Supervision, conceptualization, corresponding author, methodology, validation, funding acquisition, writing—review & editing.

Funding This study is supported by the College of Science, Department of Chemistry, Ilam University and the Central Laboratories Directorate, Iraqi Atomic Energy Commission.

Data Availability The datasets of the current study are available from the corresponding author on reasonable request.

Declarations

Conflict of interest The authors declare that they have no known competing financial interests or personal relationships that could have appeared to influence the work reported in this paper.

Ethical Approval This article does not contain any studies involving animals performed by any of the authors.

References

- W. Yao, X. Wang, Y. Liang, S. Yu, P. Gu, Y. Sun, et al. (2018). Synthesis of novel flower-like layered double oxides/carbon dots nanocomposites for U (VI) and 241Am (III) efficient removal: Batch and EXAFS studies. *Chem. Eng. J.* **332**, 775–786. <https://doi.org/10.1016/j.cej.2017.09.011>.
- Y. Sun and Y. Li (2021). Application of surface complexation modeling on adsorption of uranium at water-solid interface: A review. *Environ. Pollut.* **278**, 116861. <https://doi.org/10.1016/j.envpol.2021.116861>.
- M. Li, H. Liu, T. Chen, C. Dong, and Y. Sun (2019). Synthesis of magnetic biochar composites for enhanced uranium (VI) adsorption. *Sci. Total Environ.* **651**, 1020–1028. <https://doi.org/10.1016/j.scitotenv.2018.09.259>.
- X. Nie, X. Hu, C. Liu, X. Xia, and F. Dong (2021). Decontamination of uranium contained low-level radioactive wastewater from UO₂ fuel element industry with vacuum membrane distillation. *Desalination* **516**, 115226. <https://doi.org/10.1016/j.desal.2021.115226>.
- G. Bayramoglu, A. Akbulut, I. Acikgoz-Erkaya, and M. Y. Arica (2018). Uranium sorption by native and nitrilotriacetate-modified *Bangia atropurpurea* biomass: kinetics and thermodynamics. *J. Appl. Phycol.* **30**, 649–661. <https://doi.org/10.1007/s10811-017-1238-8>.
- R. I. Foster, J. T. Amphlett, K.-W. Kim, T. Kerry, K. Lee, and C. A. Sharrad (2020). SOHIO process legacy waste treatment: uranium recovery using ion exchange. *J. Ind. Eng. Chem.* **81**, 144–152. <https://doi.org/10.1016/j.jiec.2019.09.001>.
- J. Liao, P. Liu, Y. Xie, and Y. Zhang (2021). Metal oxide aerogels: Preparation and application for the uranium removal from aqueous solution. *Sci. Total Environ.* **768**, 144212. <https://doi.org/10.1016/j.scitotenv.2020.144212>.
- S. Li, X. Yang, Z. Cui, Y. Xu, Z. Niu, P. Li, et al. (2021). Efficient photoreduction strategy for uranium immobilization based on graphite carbon nitride/perovskite oxide heterojunction nanocomposites. *Appl. Catal. B: Environ.* **298**, 120625. <https://doi.org/10.1016/j.apcatb.2021.120625>.
- L. Kong, Y. Ruan, Q. Zheng, M. Su, Z. Diao, D. Chen, et al. (2020). Uranium extraction using hydroxyapatite recovered from phosphorus containing wastewater. *J. Hazard. Mater.* **382**, 120784. <https://doi.org/10.1016/j.jhazmat.2019.120784>.
- R. M. Al-Maliki, Q. F. Alsalhy, S. Al-Jubouri, I. K. Salih, A. A. AbdulRazak, M. A. Shehab, et al. (2022). Classification of nanomaterials and the effect of graphene oxide (GO) and

- recently developed nanoparticles on the ultrafiltration membrane and their applications: a review. *Membranes* **12** (11), 1043. <https://doi.org/10.3390/membranes12111043>.
11. F. Farivar, P. L. Yap, R. U. Karunakaran, and D. Losic (2021). Thermogravimetric analysis (TGA) of graphene materials: effect of particle size of graphene, graphene oxide and graphite on thermal parameters. *C* **7** (2), 41. <https://doi.org/10.3390/c7020041>.
 12. W. Yu, L. Sisi, Y. Haiyan, and L. Jie (2020). Progress in the functional modification of graphene/graphene oxide: A review. *RSC Adv.* **10** (26), 15328–15345. <https://doi.org/10.1039/d0ra01068e>.
 13. I. Aranaz, A. R. Alcántara, M. C. Civera, C. Arias, B. Elorza, A. Heras Caballero, and N. Acosta (2021). Chitosan: an overview of its properties and applications. *Polymers* **13** (19), 3256. <https://doi.org/10.3390/polym13193256>.
 14. A. O. Silva, R. S. Cunha, D. Hotza, and R. A. F. Machado (2021). Chitosan as a matrix of nanocomposites: A review on nanostructures, processes, properties, and applications. *Carbohydr. Polym.* **272**, 118472. <https://doi.org/10.1016/j.carbpol.2021.118472>.
 15. A. M. Omer, R. Dey, A. S. Eltaweil, E. M. Abd El-Monaem, and Z. M. Ziora (2022). Insights into recent advances of chitosan-based adsorbents for sustainable removal of heavy metals and anions. *Arab. J. Chem.* **15** (2), 103543. <https://doi.org/10.1016/j.arabjc.2021.103543>.
 16. M. Nasrollahzadeh, M. Sajjadi, S. Irvani, and R. S. Varma (2021). Starch, cellulose, pectin, gum, alginate, chitin and chitosan derived (nano) materials for sustainable water treatment: A review. *Carbohydr. Polym.* **251**, 116986. <https://doi.org/10.1016/j.carbpol.2020.116986>.
 17. D. Feldman (2020). Poly (vinyl alcohol) recent contributions to engineering and medicine. *J. Compos. Sci.* **4** (4), 175. <https://doi.org/10.3390/jcs4040175>.
 18. Y. He, H. Tian, A. Xiang, H. Wang, J. Li, X. Luo, and A. V. Rajulu (2021). Fabrication of PVA nanofibers grafted with octaamino-POSS and their application in heavy metal adsorption. *J. Polym. Environ.* **29**, 1566–1575. <https://doi.org/10.1007/s10924-020-01865-x>.
 19. M. Wang, J. Bai, K. Shao, W. Tang, X. Zhao, D. Lin, et al. (2021). Poly (vinyl alcohol) hydrogels: The old and new functional materials. *Int. J. Polym. Sci.* **2021**, 1–16. <https://doi.org/10.1155/2021/2225426>.
 20. C. I. Idumah (2021). Novel trends in polymer aerogel nanocomposites. *Polym—Plastics Technol. Mater.* **60** (14), 1519–1531. <https://doi.org/10.1080/25740881.2021.1912092>.
 21. Y. Zhao, X. Zuo, Y. Guo, H. Huang, H. Zhang, T. Wang, et al. (2021). Structural engineering of hierarchical aerogels comprised of multi-dimensional gradient carbon nanoarchitectures for highly efficient microwave absorption. *Nano-Micro Lett.* **13** (1), 144. <https://doi.org/10.1007/s40820-021-00667-7>.
 22. Y. Qin, C. Xue, H. Yu, Y. Wen, L. Zhang, and Y. Li (2021). The construction of bio-inspired hierarchically porous graphene aerogel for efficiently organic pollutants absorption. *J. Hazard. Mater.* **419**, 126441. <https://doi.org/10.1016/j.jhazmat.2021.126441>.
 23. T. T. P. N. X. Trinh, T. H. Quan, T. N. M. Anh, D. B. Thinh, N. T. Lan, D. N. Trinh, et al. (2021). Preparing three-dimensional graphene aerogels by chemical reducing method: Investigation of synthesis condition and optimization of adsorption capacity of organic dye. *Surfaces Interfaces* **23**, 101023. <https://doi.org/10.1016/j.surfin.2021.101023>.
 24. D. Zhi, T. Li, J. Li, H. Ren, and F. Meng (2021). A review of three-dimensional graphene-based aerogels: Synthesis, structure and application for microwave absorption. *Compos. Part B: Eng.* **211**, 108642. <https://doi.org/10.1016/j.compositesb.2021.108642>.
 25. N. Zaaba, K. Foo, U. Hashim, S. Tan, W.-W. Liu, and C. Voon (2017). Synthesis of graphene oxide using modified hummers method: Solvent influence. *Procedia Eng* **184**, 469–477. <https://doi.org/10.1016/j.proeng.2017.04.118>.
 26. M. C. Costa, V. S. Marangoni, P. R. Ng, H. T. Nguyen, A. Carvalho, and A. H. Castro Neto (2021). Accelerated synthesis of graphene oxide from graphene. *Nanomaterials* **11** (2), 551. <https://doi.org/10.3390/nano11020551>.
 27. E. H. Sujiono, D. Zabrian, M. Dahlan, B. Amin, and J. Agus (2020). Graphene oxide based coconut shell waste: synthesis by modified Hummers method and characterization. *Heliyon* **6** (8), e04568. <https://doi.org/10.1016/j.heliyon.2020.e04568>.
 28. S. A. Kahdestani, M. H. Shahriari, and M. Abdouss (2021). Synthesis and characterization of chitosan nanoparticles containing teicoplanin using sol–gel. *Polym. Bull.* **78**, 1133–1148. <https://doi.org/10.1007/s00289-020-03134-2>.
 29. K. Kaur, R. Jindal, and D. Saini (2020). Synthesis, optimization and characterization of PVA-co-poly (methacrylic acid) green adsorbents and applications in environmental remediation. *Polym. Bull.* **77**, 3079–3100. <https://doi.org/10.1007/s00289-019-02900-1>.
 30. W. Sun, H. Ou, and Z. Chen (2022). Study on preparation of chitosan/polyvinyl alcohol aerogel with graphene—intercalated attapulgite (GO–ATP@ CS–PVA) and adsorption properties of crystal violet dye. *Nanomaterials* **12** (22), 3931. <https://doi.org/10.3390/nano12223931>.
 31. W. Ahmed, A. Núñez-Delgado, S. Mehmood, S. Ali, M. Qaswar, A. Shakoor, and D.-Y. Chen (2021). Highly efficient uranium (VI) capture from aqueous solution by means of a hydroxyapatite-biochar nanocomposite: adsorption behavior and mechanism. *Environ. Res.* **201**, 111518. <https://doi.org/10.1016/j.envres.2021.111518>.
 32. Y. Li, A. O. Simon, C. Jiao, M. Zhang, W. Yan, H. Rao, et al. (2020). Rapid removal of Sr²⁺, Cs⁺ and UO₂²⁺ from solution with surfactant and amino acid modified zeolite Y. *Micropor. Mesopor. Mater.* **302**, 110244. <https://doi.org/10.1016/j.micromeso.2020.110244>.
 33. S. Zhou, F. Dong, and Y. Qin (2023). High efficiency uranium (VI) removal from wastewater by strong alkaline ion exchange fiber: Effect and characteristic. *Polymers* **15** (2), 279. <https://doi.org/10.3390/polym15020279>.
 34. Y. Liu, Y. Chen, H. Zhao, and C. Teng (2021). Characterization, dielectric properties, and mechanical properties of cyanate epoxy composites modified by KH550-ALOOH@ GO. *J. Mater. Sci.: Mater. Electron.* **32**, 8890–8902. <https://doi.org/10.1007/s10854-021-05561-x>.
 35. M. S. K. Sofla, S. Mortazavi, and J. Seyfi (2020). Preparation and characterization of polyvinyl alcohol/chitosan blends plasticized and compatibilized by glycerol/polyethylene glycol. *Carbohydr. Polym.* **232**, 115784. <https://doi.org/10.1016/j.carbpol.2019.115784>.
 36. A. V. Maffei, P. M. Budd, and N. B. McKeown (2006). Adsorption studies of a microporous phthalocyanine network polymer. *Langmuir* **22** (9), 4225–4229. <https://doi.org/10.1021/la06091z>.
 37. Z. Wang, D. Zhao, C. Wu, S. Chen, Y. Wang, and C. Chen (2020). Magnetic metal organic frameworks/graphene oxide adsorbent for the removal of U(VI) from aqueous solution. *Appl. Radiat. Isotopes* **162**, 109160. <https://doi.org/10.1016/j.apradiso.2020.109160>.
 38. X. Liu, J. Sun, X. Xu, A. Alsaedi, T. Hayat, and J. Li (2019). Adsorption and desorption of U (VI) on different-size graphene oxide. *Chem. Eng. J.* **360**, 941–950. <https://doi.org/10.1016/j.cej.2018.04.050>.

39. M. A. Al-Ghouti and D. A. Da'ana (2020). Guidelines for the use and interpretation of adsorption isotherm models: a review. *J. Hazard. Mater.* **393**, 122383. <https://doi.org/10.1016/j.jhazmat.2020.122383>.

Publisher's Note Springer Nature remains neutral with regard to jurisdictional claims in published maps and institutional affiliations.

Springer Nature or its licensor (e.g. a society or other partner) holds exclusive rights to this article under a publishing agreement with the author(s) or other rightsholder(s); author self-archiving of the accepted manuscript version of this article is solely governed by the terms of such publishing agreement and applicable law.